SPECIAL
PANDOWAE
COLLECTION

Enhanced Tropospheric Wave Forcing of Two Anticyclones in the Prephase of the January 2009 Major Stratospheric Sudden Warming Event

ANDREA SCHNEIDEREIT AND DIETER H. W. PETERS

Leibniz-Institute of Atmospheric Physics, University of Rostock, Kühlungsborn, Germany

CHRISTIAN M. GRAMS AND JULIAN F. QUINTING[a]

Institute for Atmospheric and Climate Science, ETH Zürich, Zurich, Switzerland

JULIA H. KELLER[b]

Deutscher Wetterdienst, Offenbach, Germany

GABRIEL WOLF,[c] FRANZISKA TEUBLER, AND MICHAEL RIEMER

Institute for Atmospheric Physics, Johannes Gutenberg-University, Mainz, Germany

OLIVIA MARTIUS

Mobiliar Lab for Natural Risk, Oeschger Centre for Climate Change Research, Institute of Geography, University of Bern, Bern, Switzerland

(Manuscript received 27 June 2016, in final form 17 January 2017)

ABSTRACT

Tropospheric forcing of planetary wavenumber 2 is examined in the prephase of the major stratospheric sudden warming event in January 2009 (MSSW 2009). Because of a huge increase in Eliassen–Palm fluxes induced mainly by wavenumber 2, easterly angular momentum is transported into the Arctic stratosphere, deposited, and then decelerates the polar night jet. In agreement with earlier studies, the results reveal that the strongest eddy heat fluxes, associated with wavenumber 2, occur at 100 hPa during the prephase of MSSW 2009 in ERA-Interim. In addition, moderate conditions of the cold phase of ENSO (La Niña) contribute to the eddy heat flux anomaly. It is shown that enhanced tropospheric wave forcing over Alaska and Scandinavia is caused by tropical processes in two ways. First, in a climatological sense, La Niña contributes to an enhanced anticyclonic flow over both regions. Second, the Madden–Julian oscillation (MJO) has an indirect influence on the Alaskan ridge by enhancing eddy activity over the North Pacific. This is manifested in an increase in cyclone frequency and associated warm conveyor belt outflow, which contribute to the maintenance and amplification of the Alaskan anticyclone. The Scandinavian ridge is maintained by wave trains emanating from the Alaskan ridge propagating eastward, including an enhanced transport of eddy kinetic energy. The MSSW 2009 is an extraordinary case of how a beneficial phasing of La Niña and MJO conditions together with multiscale interactions enhances tropospheric forcing for wavenumber 2–induced zonal mean eddy heat flux in the lower stratosphere.

Supplemental information related to this paper is available at the Journals Online website: http://dx.doi.org/10.1175/MWR-D-16-0242.s1.

[a] Current affiliation: School of Earth, Atmosphere and Environment, Monash University, Clayton, Victoria, Australia.
[b] Current affiliation: World Meteorological Organization, Geneva, Switzerland.
[c] Current affiliation: University of Reading, Reading, United Kingdom.

Corresponding author e-mail: Andrea Schneidereit, schneidereit@iap-kborn.de

DOI: 10.1175/MWR-D-16-0242.1

1. Introduction

During a stratospheric sudden warming (SSW) event, the polar stratospheric temperature increases accompanied by a weakening of the polar night jet. Major SSW events (MSSW) are defined as SSW events with a reversal of the zonal mean zonal wind from westerlies to easterlies at 60°N and a 10-hPa layer. Those events represent the greatest part of intraseasonal variability in the winter middle atmosphere and are associated with low predictive skill at lead times more than 10 days (Tripathi et al. 2015). Matsuno (1971) developed a dynamical model of the stratospheric sudden warming phenomena in which tropospheric forced planetary wave packets propagate upward into the stratosphere. The deposition of their easterly angular momentum [Eliassen–Palm flux (EP flux) convergence] leads to a weakening and breakdown of the polar night jet.

Several processes influence the occurrence of MSSW events in the Northern Hemisphere: the quasi-biennial oscillation (QBO) and the solar cycle (e.g., Labitzke 1987; van Loon and Labitzke 1987), zonally asymmetric ozone changes (e.g., Peters et al. 2015), El Niño–Southern Oscillation (ENSO) (e.g., Butler and Polvani 2011), and the Madden–Julian oscillation (MJO) (e.g., Garfinkel et al. 2012; Liu et al. 2014). All these processes change the forcing of planetary waves in the troposphere or change the wave propagation into and in the stratosphere (mainly wavenumbers 1–3; Charney and Drazin 1961; Dickinson 1969). The strong mean-flow deceleration in the stratosphere during an MSSW event is mainly caused by an amplification of linear waves in the troposphere and their upward propagation into the stratosphere, which induces a negative vertical gradient of the meridional eddy heat flux (EP flux convergence) (Holton 1992).

Under the acting Eliassen–Palm flux convergence, the polar vortex breaks down (e.g., Andrews et al. 1987). Generally, the divergence of the EP flux represents a zonal force on the mean state by the disturbances (Edmon et al. 1980). Furthermore, it can be shown following the generalized Eliassen–Palm theorem that the poleward zonal mean eddy heat flux is proportional to the vertical group velocity of linear planetary waves. A measure of wave activity entering the stratosphere is the zonal mean eddy heat flux at 100 hPa (Waugh et al. 1999; Polvani and Waugh 2004), because it is proportional to the vertical component of the EP flux (Andrews et al. 1987). Although both the zonal mean eddy heat flux at 100 hPa and the upper-stratospheric convergence of the EP flux are highly correlated, the meridional derivative of the zonal mean eddy momentum flux also contributes (Newman et al. 2001). Both the zonal mean eddy momentum flux and the eddy heat flux act together. However, the zonal mean eddy heat flux is used in this paper as a proxy to evaluate the role of tropospheric forcing processes of planetary waves and as a quantitative measure of wave propagation across the tropopause region.

Several studies show that tropospheric processes like blocking anticyclones in the extratropics and like ENSO and MJO in the tropics influence the preconditioning of the polar vortex in advance of an MSSW event. Barriopedro and Calvo (2014) studied the relationship between ENSO, MSSWs, and blocking. They show that during the cold phase of ENSO (La Niña), blocking anticyclones frequently occur over the eastern Pacific and over the Scandinavian–Kara Sea region before MSSW events. Under mean La Niña conditions, MSSW events are predominantly linked to a wavenumber-2 amplification. MSSW polar vortex splitting events, as occurred in January 2009, are typically preceded by tropospheric blocking either over the Pacific sector alone or over both the Euro-Atlantic and Pacific sectors collocated with a wavenumber-2 pattern (e.g., Martius et al. 2009).

Besides the influence of ENSO, the MJO is known to force in the form of tropical convection and upper-level divergence anomalous Rossby wave breaking over the North Pacific, which is linked with enhanced cyclone frequency (Moore et al. 2010). This modulates the eddy heat flux, which is in phase with the climatological planetary waves (Garfinkel et al. 2014). Ferranti et al. (1990) show that the MJO influences the planetary wave structure significantly in extratropical midlatitudes. The MJO teleconnection pattern of phases 7 and 8 (Wheeler and Hendon 2004) are preferentially linked to a low pressure anomaly over the central North Pacific and high pressure over Canada (Garfinkel et al. 2012). If the resulting quasi-stationary trough–ridge pattern is in phase with the climatological ultralong waves, then an increase of the upward tropospheric wave forcing is expected. In this way the MJO enhances the upward-propagating planetary waves in the extratropics. Liu et al. (2014) examine the mechanisms for the influence of MJO on splitting or displacement MSSW events and find that MJO-related circulation patterns, occurring during phases 7 and 8, are often associated with vortex-split MSSWs. Note that MJO-related anomalies over high latitudes vary with ENSO (Roundy et al. 2010). If both La Niña and MJO phase 7 are present, then the Canadian trough, the ridge over Europe, and the trough over Asia are amplified and occur with higher amplitudes compared to La Niña–only composites.

From a more synoptic perspective, extratropical trough–ridge patterns are often associated with strong diabatic processes that influence the patterns themselves and the evolution of the downstream flow (e.g., Davis et al. 1993; Grams et al. 2011). The most intense latent

heating occurs in the warm sector of the cyclone in so-called warm conveyor belts (WCBs, Carlson 1980).

Ascent within these vigorous cross-isentropic airstreams leads to a net transport of lower-tropospheric air with low Ertel potential vorticity (PV; Ertel 1942) into the upper troposphere. Recent research highlights that the resulting upper-level outflow of such airstreams is important for the amplification of Rossby waves in the upper troposphere and for the onset of blocking anticyclones (Pfahl et al. 2015; Grams and Archambault 2016; Teubler and Riemer 2016).

In January 2009 a very strong MSSW (MSSW 2009) was observed with a splitting of the polar vortex. This event occurred with one of the largest zonal mean eddy heat fluxes at 100 hPa ever observed until that date since 1958 (Ayarzagüena et al. 2011).

In the present study, the central date (CD) of the MSSW event is defined as the day before the reversal of the zonal mean zonal wind at 60°N and at 10 hPa: identified on 23 January 2009 by using the polar cap–averaged geopotential height anomaly method (central dates of the MSSW events are listed in Table TS1 in the online supplemental material). Note that the specific CD changed only slightly when using different methods (Butler et al. 2015).

For MSSW 2009, the upper-tropospheric ridge over Alaska is of particular importance (Harada et al. 2010; Ayarzagüena et al. 2011). Upward wave energy propagation, which starts roughly 10 days before the CD, is mainly concentrated close to the ridge over Alaska and is weaker to the east of the Scandinavian ridge (Harada et al. 2010) but stronger, as known from mean climatologies. This event occurred along with an intense polar night jet oscillation with a strong negative northern annular mode in the stratosphere (Hitchcock et al. 2013) and had strong impacts on the polar middle atmosphere (Pedatella et al. 2014) and on the troposphere after the breakdown of the polar vortex. Hinssen et al. (2011) show a strong and long-lasting zonal mean zonal wind deceleration in the troposphere that is directly linked to the polar vortex breakdown in January 2009.

The warming occurred despite the QBO (westerly monthly mean zonal wind of about 14 $m\,s^{-1}$ at 40 hPa and about 12 $m\,s^{-1}$ at 50 hPa[1]) and solar cycle pointing toward a stable cold polar vortex (Labitzke and Kunze 2009). Therefore, favorable tropical conditions like ENSO or MJO may have been responsible for the occurrence of the MSSW 2009. During the prephase of the MSSW (here defined as 10-day period before the CD), moderate La Niña conditions and an active MJO prevailed in the tropical Pacific.

In this study, we aim to reveal the role of La Niña and the MJO in increasing the zonal mean eddy heat flux at 100 hPa during the prephase of the MSSW 2009. The primary open question to be addressed is as follows: How do these tropical modes—La Niña and active MJO phases 7 and 8—influence the midlatitudes and, especially, influence the zonal mean eddy heat flux increase at 100 hPa? The focus lies on the prephase, which is characterized by a large increase in wavenumber-2 amplitude of the meridional wind ($v^\star$, where the superscript star indicates the deviation from zonal mean) in comparison to wavenumbers 1 and 3. This paper analyzes in a novel approach which tropospheric processes contribute to the amplification of the Alaskan and Scandinavian anticyclones and hence to wavenumber 2 prior to the CD and the induced zonal mean eddy heat flux.

After a brief description of the data and methods used, the study examines the increase of the zonal mean eddy heat fluxes as a function of anomalies and La Niña climatology. Furthermore, the enhanced tropospheric wave forcing of ridges over Alaska and Scandinavia is investigated. We expect that La Niña and MJO have an indirect influence on the ridge over Alaska. In addition, anomalies of cyclone frequency and WCB activity over the North Pacific are examined to reveal their contribution to the observed development of the anticyclone. The mechanisms of the amplification of the Alaskan and Scandinavian anticyclones are diagnosed next. The article is finalized by a summary.

2. Data and methods

a. Data

The ERA-Interim data of the European Centre for Medium-Range Weather Forecasts are used (Dee et al. 2011). The present analysis includes the period from 1979 to 2012. If not stated otherwise, daily data are used on a horizontal grid of 2.5° × 2.5° resolution. Often a 5-day running mean is applied in order to smooth out high-frequency variability. This is indicated in the figure captions.

The monthly ENSO index stems from the National Oceanic and Atmospheric Administration (NOAA)'s Climate Prediction Center (CPC)[2] and is used to classify La Niña Januaries. A January belongs to La Niña (El Niño) if the monthly Niño-3.4 index is below (above)

[1] http://www.geo.fu-berlin.de/en/met/ag/strat/produkte/index.html#compilation.

[2] http://www.cpc.ncep.noaa.gov/products/analysis_monitoring/ensostuff/detrend.nino34.ascii.txt.

one standard deviation of the entire monthly time series (1950–2012). The following La Niña Januaries are used: 1985, 1989, 1996, 1999, 2000, 2006, 2008, 2009, 2011, and 2012. In winter 2008/09, the monthly Niño-3.4 index is about −0.7, −0.9, and −0.75 for December–February, respectively. Composites of cyclone frequency anomaly under La Niña–only conditions are evaluated for the climatological prephase 2–23 January.

The MJO life cycle is divided into eight phases using the Real-time Multivariate MJO (RMM) indices of Wheeler and Hendon (2004).[3] Only days with an RMM amplitude (defined as $\sqrt{\text{RMM1}^2 + \text{RMM2}^2}$) greater than 1 are used. MJO phase composites of cyclone frequency anomaly are calculated relative to the December–February 1980–2010 climatological mean. Composites with the simultaneous occurrence of La Niña (10 winters) and MJO active phases 7 and 8 (Figs. 6c and 6d, respectively) consider means over 94 and 74 days, respectively.

b. Methods

Several methods are applied in order to examine the tropospheric forcing during La Niña and MJO phases over the North Pacific Ocean, in particular, and farther downstream in the Atlantic–European sector, and to understand their contribution to the amplification of the anticyclones. Furthermore, tendency equations of eddy kinetic energy K_e and Ertel's PV (Ertel 1942) are evaluated to quantify the forcing mechanisms of ridges. The standard approaches of Plumb (1985) and Takaya and Nakamura (1997) are used to diagnose wave activity fluxes. Also, classical EP flux calculations (Andrews et al. 1987) for different wavenumbers and different bandpass filters are performed.

1) Cyclone frequency

Cyclones are identified in global 6-hourly data at 1° horizontal resolution using a modified version of the cyclone identification and tracking scheme of Wernli and Schwierz (2006). A cyclone is identified in the sea level pressure (SLP) field as a minimum with an enclosing isobar. This closed isobar determines the area of a cyclone. The difference between the isobar and the closed SLP minimum must be at least 1 hPa. The upper bound for the length of the isobar is 7500 km. Only SLP minima are considered in regions with orography below 1500 m. More details can be found in Pfahl and Wernli (2012). The cyclone frequency at a specific grid point indicates the percentage of days during a considered period with a cyclone at this grid point.

[3] http://www.bom.gov.au/climate/mjo/graphics/rmm.74toRealtime.txt.

2) Warm conveyor belts

The WCBs discussed in this study are extracted from the climatology of Madonna et al. (2014) based on global 6-hourly ERA-Interim data at 1° horizontal resolution. WCBs are selected from 2-day forward LAGRANTO (Sprenger and Wernli 2015) hPa trajectories (t = 0–48 h, every 6 h), started from equally distributed locations every 20 in a layer from 1050 to 790 hPa (above orography only). WCBs must ascend at least 600 hPa within 2 days (48 h) and have to be located near an extratropical cyclone. The last criterion is fulfilled by the condition that WCB trajectories must pass the area of an extratropical cyclone at least once during their lifetime. The cyclone area is the area defined by the closed isobar, used in the cyclone identification method. WCB parcel locations at $t = 0$ (inflow), t = 48 (outflow), and t = 0–48 h (entire WCB lifetime) are gridded onto a regular geographical grid every 6 h.

3) Eddy kinetic energy

Orlanski and Katzfey (1991) derive Eq. (1) for the local tendency in K_e. A detailed description and examples of K_e propagation can be found also in Orlanski and Sheldon (1995); the equation for the local tendency of K_e reads as follows:

$$\frac{\partial K_e}{\partial t} = -(\mathbf{v}' \cdot \nabla\phi') - \nabla \cdot (\mathbf{V}K_e) - \frac{\partial(\omega' K_e)}{\partial p} - \mathbf{v}' \cdot (\mathbf{v}' \cdot \nabla\overline{\mathbf{V}}) + R, \tag{1}$$

where ϕ is the geopotential; $\mathbf{V}$ is the horizontal wind vector, which is partitioned into perturbation and time mean ($\mathbf{V} = \mathbf{v}' + \overline{\mathbf{V}}$); and ω' is the vertical velocity. Primes denote perturbations, which are defined as deviations from a 30-day running mean, centered on the date of investigation. The time mean is indicated by an overbar. According to Eq. (1), the tendency of K_e results from the work done by pressure forces [first term on the rhs of Eq. (1)], the horizontal and vertical advection of K_e by the total wind (second and third terms, respectively), the barotropic interaction between eddy and mean flow (fourth term), and some residual (e.g., friction). The first term on the rhs can also be expressed as

$$-\mathbf{v}' \cdot \nabla\phi' = -\omega'\alpha - \nabla \cdot (\mathbf{v}'\phi')_a - \frac{\partial(\omega'\phi')}{\partial p}, \tag{2}$$

where α is the specific volume, defined as $\alpha = \partial\phi/\partial p$, and $(\mathbf{v}'\phi')_a$ is the geopotential fluxes with most of the nondivergent part removed (Orlanski and Sheldon 1995). The work done by pressure forces equals the baroclinic conversion [first term on the rhs of Eq. (2)] and the divergence of the ageostrophic geopotential flux (second and third terms), which can also be described as a

dispersive K_e flux. The baroclinic conversion describes the conversion from eddy available potential energy into K_e and vice versa. All quantities are vertically integrated between 1000 and 100 hPa and are normalized by the gravitational acceleration.

4) PV TENDENCY

Based on the concept of baroclinically coupled Rossby waves (Ertel 1942; Hoskins et al. 1985) and their downstream development (Simmons and Hoskins 1979), a quantitative PV framework was developed (Teubler and Riemer 2016) and applied previously to the evolution of a large-amplitude ridge associated with a severe precipitation event (Piaget et al. 2015). The hydrostatic form of Ertel's potential vorticity on an isentropic surface $\mathrm{PV} = \sigma^{-1}(\zeta + f)$ is used, where ζ is the vertical component of relative vorticity on an isentropic surface, f is the Coriolis parameter, $\sigma^{-1} = g\partial\theta/\partial p$, g is the gravity acceleration, p is pressure, and θ is potential temperature. The framework is based on the PV tendency equation spatially integrated over an area of interest, here: the Alaskan ridge. The ridge itself is defined as a roughly persistent (here: 14 days) and spatial coherent negative anomaly of Ertel's PV on isentropes intersecting the tropopause (here: 320–330 K). Anomalies in PV, PV′, are defined as a deviation from a 60-day average centered on the CD. A 60-day background flow is chosen because the Alaskan ridge is more persistent than the high-frequency eddies. The PV diagnostic is performed with the Year of Tropical Convection (YOTC) dataset using a $1° \times 1°$ horizontal grid resolution.

The advective contribution is partitioned, using piecewise PV inversion and Helmholtz partitioning, into $\mathbf{v} = \mathbf{v}_{\mathrm{bg}} + \mathbf{v}_{\mathrm{qb}} + \mathbf{v}_{\mathrm{bc}} + \mathbf{v}_{\mathrm{div}}$. The index bg denotes the background flow and the index div indicates the divergent part of the wind. Contributions from PV anomalies below and above 650 hPa are referred to as baroclinic (index bc) and quasi barotropic (index qb). Note that since $\mathbf{v}_{\mathrm{bg}} \cdot \nabla\overline{\mathrm{PV}} \approx 0$, the impact of the background flow vanishes. The evolution of the ridge is described in terms of the total tendency of the area-integrated amplitude of PV anomaly, which is given by

$$\frac{d}{dt}\int_{\mathscr{A}(t)} \mathrm{PV}'\, dA = -\int_{\mathscr{A}} [\mathbf{v}_{\mathrm{qb}} \cdot \nabla\overline{\mathrm{PV}} + \mathbf{v}_{\mathrm{bc}} \cdot \nabla\overline{\mathrm{PV}} + \mathrm{PV}(\nabla \cdot \mathbf{v}_{\mathrm{div}}) - \mathrm{DIA}]\, dA + \mathscr{R}, \qquad (3)$$

where $\mathbf{v}$ is the horizontal wind vector on an isentropic surface and $\overline{\mathrm{PV}}$ is the background PV field. Nonadvective tendencies due to diabatic processes with contributions from latent heat release are designed by DIA. Term $\mathscr{R}$ indicates the residual term, which contains boundary contributions and frictional processes, and is considered to be small (Teubler and Riemer 2016). Term $\mathscr{A}$ refers here to the integration area of the Alaskan ridge.

The advective tendencies can be interpreted as follows: The quasi-barotropic tendency is associated with the group propagation of Rossby wave packets and is similar to the divergence of the ageostrophic geopotential flux from the K_e analysis. The baroclinic tendency signifies baroclinic interaction between the upper- and lower-level anomalies (e.g., baroclinic growth). The divergent flow at upper levels can be predominantly associated with latent heat release below (cf. also Riemer et al. 2014) and thus can be interpreted as having an indirect diabatic impact on the ridge. A comprehensive comparison of the PV tendency framework and the more commonly used K_e framework can be found in Teubler and Riemer (2016). Together with the diabatic contribution, the ridge evolution is then governed by four different processes.

5) WAVE ACTIVITY FLUX

The wave activity flux (WAF) is calculated in two different ways. First, to analyze the climatological stationary waves, the WAF is calculated according to Plumb (1985). Deviations from this climatology are identified by WAF for the extended prephase (1–23 January 2009). Second, the WAF according to Takaya and Nakamura (1997) is calculated using the following bandpass-filtered data: (i) transient (high-pass filter of 1–6 days for the perturbation of low-pass-filtered background with 10 days and larger); (ii) intermediate (bandpass filter between 8 and 20 days for the perturbations from low-pass-filtered background with 30 days and larger); and (iii) quasi planetary (bandpass filter of 20–60 days for the deviations, low-pass filter of 60 days and larger for the background flow). Note that the basic flow is zonally uniform for WAF according to Plumb (1985) and is zonally varying for WAF according to Takaya and Nakamura (1997). Plumb (1985) considered stationary perturbations (perturbations from zonal mean), while Takaya and Nakamura (1997) considered perturbations against the steady horizontal, nondivergent zonally dependent basic flow. Hence, perturbations in Takaya and Nakamura (1997) can be regarded as migratory disturbances rather than stationary waves. Both fluxes reduce to the EP flux if stationary waves, zonal averages, and a zonally uniform basic flow are considered. All these fluxes help to understand the wave–mean flow interaction, by analyzing their vector field (energy propagation) and their divergence (changes in background flow).

3. Results

a. *Eddy heat flux from wavenumber 2 and La Niña*

The zonal mean zonal wind at 10 hPa and 60°N starts to decrease about 14 days before the CD, mainly caused

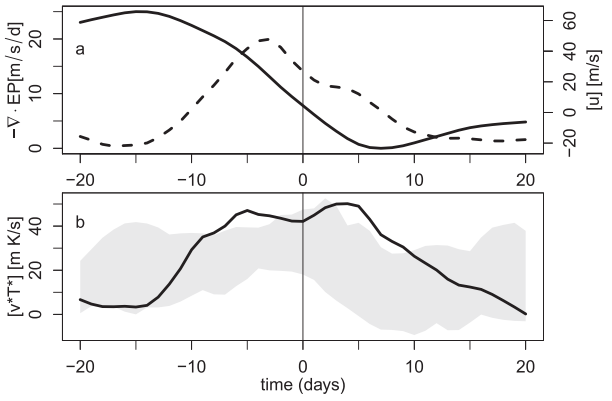

FIG. 1. Temporal evolution of (a) zonal mean zonal wind at 60°N (solid line, right axis) and the convergence of EP flux (dashed line, left axis) averaged between 45° and 75°N, both at 10 hPa; and (b) zonal mean eddy heat flux averaged over 45°–75°N at 100 hPa (black line), shown as a 5-day running mean. Shading in (b) denotes the climatological extreme variability of $[v^\star T^\star]$ of MSSW events around CD (included are MSSWs prior to 2009 in the ERA-Interim period, in total 17 MSSWs). The vertical line at zero indicates CD. For MSSW 2009, the CD is around 23 Jan 2009. The x axis is relative centered around CD. All considered MSSW events in (b) are listed in Table TS1.

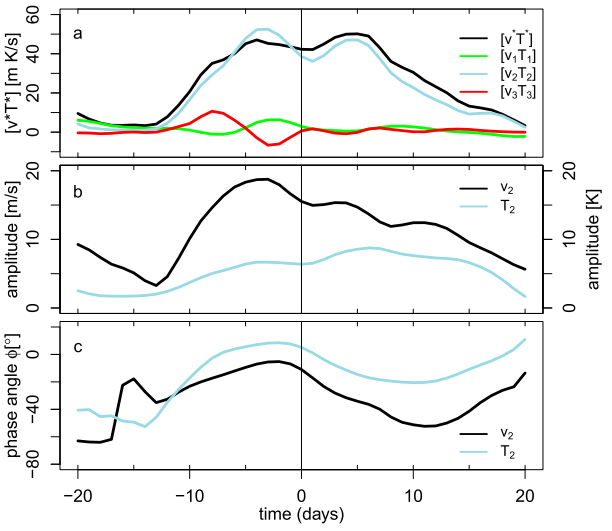

FIG. 2. (a) Zonal mean eddy heat flux averaged between 45° and 75°N at 100 hPa (black line) and separately for wave components for wavenumbers 1–3 (green, blue, and red, respectively). The vertical line indicates the CD of MSSW 2009. Mean (b) amplitude and (c) phase of wavenumber-2 components for meridional wind v_2 and temperature T_2. A 5-day running mean is applied before harmonic analysis.

by the EP flux convergence (Fig. 1a), in agreement with classical theory and observations of Harada et al. (2010) and Ayarzagüena et al. (2011). As can be seen from Fig. 1, the divergence of the EP flux is not the only force that acts on the temporal change of the zonal mean zonal wind. For example, 5 days before the CD, the convergence of the EP flux is roughly $20\,\mathrm{m\,s^{-1}\,day^{-1}}$. At the same time, $d[u]/dt$ is roughly $7\,\mathrm{m\,s^{-1}\,day^{-1}}$, which illustrates that the Coriolis term has a counteracting impact. The strong correlation of $r = 0.79$ between EP flux convergence at 10 hPa (Fig. 1a) and zonal mean eddy heat flux at 100 hPa (Fig. 1b) is also confirmed, which explains about 62% of variance (Newman et al. 2001). Furthermore, as shown by Harada et al. (2010) and Ayarzagüena et al. (2011), the zonal mean eddy heat flux ($[v^\star T^\star]$, where the superscript star indicates the deviation from the zonal mean and $[\cdots]$ indicates the zonal mean) at 100 hPa averaged over a latitudinal belt from 45° to 75°N reveals one of the largest zonal mean eddy heat fluxes at 100 hPa ever observed in the prephase of MSSWs until that date (Fig. 1b). Days of comparable strong zonal mean eddy heat fluxes at 100 hPa occur in Januaries of 1979, 1987, 1995, and 2010. All these Januaries do not belong to the group of La Niña events. A maximum of the total zonal mean eddy heat flux occurs after the CD, which may be linked with internal processes (wave–mean flow or wave–wave interaction) of the stratosphere as discussed by Albers and Birner (2014). Because we are interested in the prephase of MSSW 2009, only the first peak (Fig. 1b) will be analyzed in more detail, which occurs around 5 days prior to the CD.

The first peak of $[v^\star T^\star]$ arises mainly from wavenumber 2 (Fig. 2a). Other wavenumbers show only marginal contributions in the prephase. Because the wavenumber-2 contribution maximizes in the prephase, only the wavenumber-2 amplitude and phase evolution are considered in the following (Figs. 2b and 2c, respectively). The temporal evolution of the amplitude of the wavenumber-2 meridional wind v_2 and the wavenumber-2 temperature T_2 shows that in particular the increase of the amplitude of v_2 is stronger than the increase of the amplitude of T_2 during the prephase (Fig. 2b). Hence, the increase in amplitude of wavenumber 2 in v_2 and (minor) in T_2 mainly contributes to the wavenumber 2–induced zonal mean eddy heat flux because the phasing (Fig. 2c) between both, v_2 and T_2, is nearly constant (about 20°). There are two phase jumps before the 10-day prephase and a slight increase during the postphase. Under geostrophic balance, v is simply proportional to the longitudinal gradient of the geopotential and T is proportional to the vertical gradient of the geopotential. Hence, the first peak of the zonal mean eddy heat flux (before CD; Fig. 2a) results mainly from a horizontal amplification of the wavenumber-2 pattern at about 100 hPa and below (Fig. 3). The strengthening of the two ridges occurs simultaneously with the increase of the zonal mean eddy heat flux at 100 hPa. Note the second peak (after CD; Fig. 2a) results mainly from the product

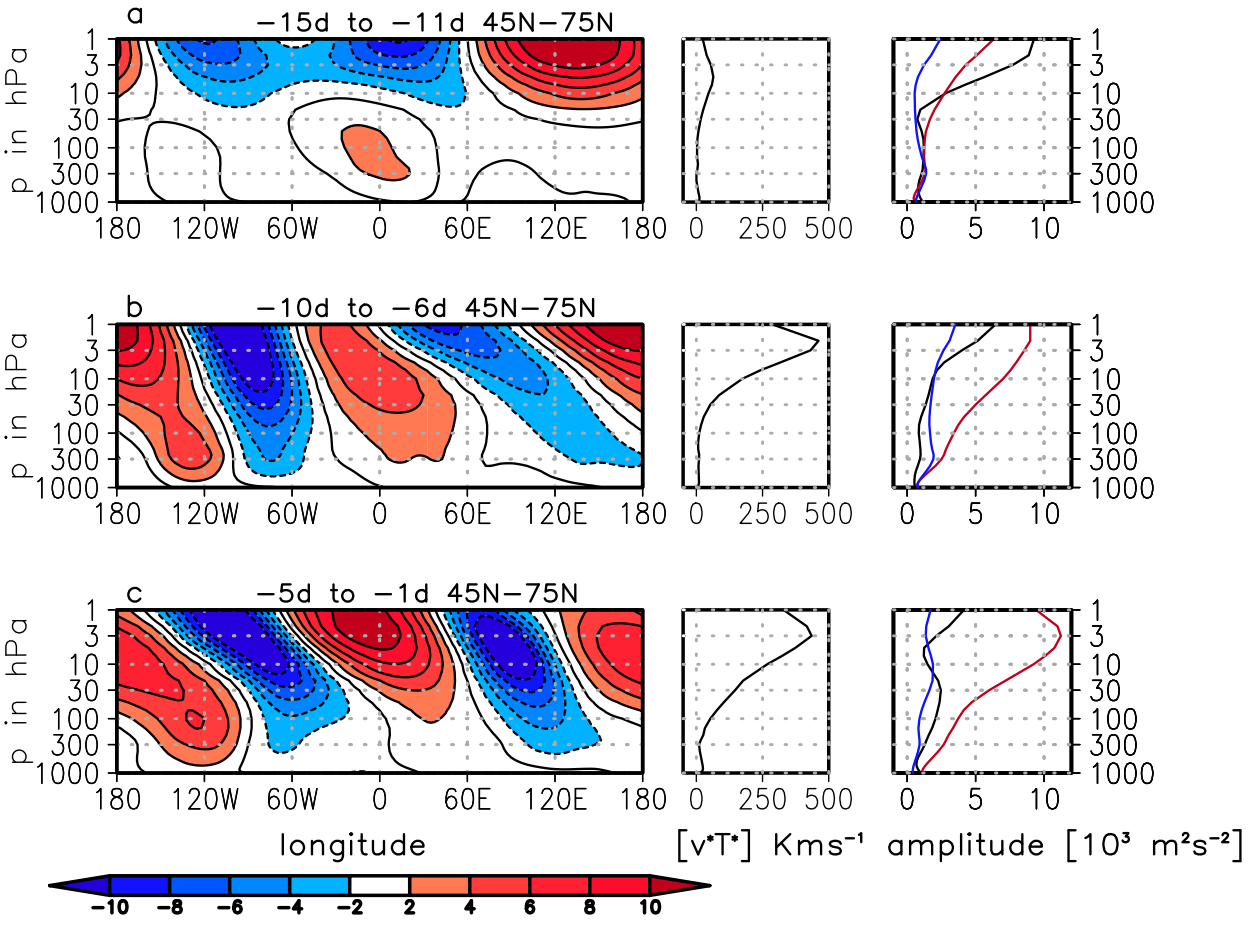

FIG. 3. (left) Pressure–longitude cross sections of total geopotential disturbance ($10^3\,m^2\,s^{-2}$) averaged between 45° and 75°N and 5-day means for the (a) 15–11 days before CD, (b) 10–6 days before CD, and (c) 5 days–1 day before CD. Vertical profiles of the (middle) zonal mean eddy heat flux and (right) geopotential amplitudes of wavenumber 1 (black), wavenumber 2 (red), and wavenumber 3 (blue) averaged between 45° and 75°N for the corresponding 5-day means.

of a moderate v_2 and the largest temperature amplitude T_2. This can be related to an increase of the vertical gradient of the geopotential at 100 hPa and reflects the differential vertical propagation of wavenumber 2.

The evolution of the zonal mean eddy heat flux components reveals the main contribution from wavenumber-2 amplitude about 10 days before CD, which is confirmed by harmonic analysis showing the dominance of wavenumber-2 amplitude in comparison to the amplitude of wavenumbers 1 and 3 (shown in Fig. S1 in the supplemental material). The vertical and temporal evolution of the 5-day mean geopotential disturbance (Fig. 3; *disturbance* is defined as a deviation from zonal mean) indicates a strong increase of the disturbances during the subperiod of 10–6 days before the CD. In comparison to the 5-day period before (15–11 days before the CD), the Alaskan ridge strengthens about $4500\,m^2\,s^{-2}$ at 100 hPa, while the Scandinavian ridge strengthens about $1000\,m^2\,s^{-2}$ during the subperiod of 10–6 days before the CD. This is followed by an upward propagation of the centers of the geopotential disturbances, in particular the center of the Scandinavian ridge during the subperiod of 5–1-day period before the CD. The stronger upward propagation is indicated by a stronger westward tilt of the geopotential extrema with height. A harmonic analysis of the 5-day averaged geopotential disturbances (Fig. 3, right panel) further illustrates the strengthening of the wavenumber-2 amplitude.

As mentioned before, two anticyclones occur, one over the midlatitudes over the Gulf of Alaska at about 120°W and the other over Scandinavia at about 30°E (Fig. 3). The superposition of the ultralong waves (wavenumbers 1–3) alone shows a strengthening and an amplification of the anticyclone over the Gulf of Alaska during the subperiod of 10–6 days before CD, while the anticyclone over Europe amplifies and strengthens during the subperiod of 5–1 day before CD (shown in Fig. S1). The strengthening of the two anticyclones supports the

TABLE 1. Zonal mean eddy heat flux (K m s^{-1}) at 100 hPa averaged between 50° and 80°N for the ultralong planetary waves, corresponding to the period 16–20 Jan 2009, and the decomposition of $[v^\star T^\star]$ into climatological and anomalous contributions.

Wavenumbers	$[v^\star T^\star]$	$[v_a^\star T_a^\star]$	%	$[v_c^\star T_c^\star]$	%	$[v_a^\star T_c^\star]$	%	$[v_c^\star T_a^\star]$	%
1–3	59	36	61	12	20	11	19	0	0
1	6	2		7		1		−4	
2	55	35	59	4	7	12	20	4	7
3	−2	−1		1		−2		0	

finding that wavenumber 2 dominates the dynamical behavior during the prephase of the MSSW 2009 event in the troposphere and stratosphere.

Through a decomposition of $[v^\star T^\star]$ into climatological (daily climatology, index c) and anomalous parts (index a), Ayarzagüena et al. (2011) show that during the prephase of MSSW 2009, the first peak or maximum of $[v^\star T^\star]$ is mainly determined by anomalies of ultralong waves (accounting for more than 63% of the whole $[v^\star T^\star]$ peak). The correlation between anomalous and climatological waves $[v_a^\star T_c^\star]$ and between both climatological waves $[v_c^\star T_c^\star]$ still contributes to $[v^\star T^\star]$ with 17% and 19%, respectively (Ayarzagüena et al. 2011, their Table 1). The climatological zonal mean eddy heat flux is dominated by a wavenumber-1 contribution, while the contributions of the anomalous zonal mean eddy heat flux $[v_a^\star T_a^\star]$ and the cross correlation $[v_a^\star T_c^\star]$ arise mainly from wavenumber 2. To examine the contribution of La Niña to the zonal mean eddy heat flux of January 2009, $[v^\star T^\star]$ is decomposed into climatological and anomalous wave contributions in accordance with Nishii et al. (2009). Note that the same time filtering is applied to the data as described by Ayarzagüena et al. (2011). The use of ERA-Interim data reveals only minor differences in the zonal mean eddy heat fluxes in comparison to the NCEP–NCAR reanalysis used by Ayarzagüena et al. (2011). The anomalous zonal mean eddy heat flux of ultralong waves $[v_a^\star T_a^\star]$ contributes mainly (about 61%; Table 1, first row) to the first peak of $[v^\star T^\star]$ (Fig. 2a), weaker contributions come from the $[v_c^\star T_c^\star]$ term with about 20%, and from the $[v_a^\star T_c^\star]$ term with about 19%. The $[v_c^\star T_a^\star]$ contribution is about zero. The dominant contributions are shown by wavenumber-2 components (Table 1, third row) for the correlation.

In comparison to climatology (discussed above), mean La Niña climatology results are similar except for wavenumber 2 (Table 2). The contribution of $[v_a^\star T_c^\star]$ for wavenumber 2 shows a contribution of 25%, indicating an increase of 5% in comparison to climatology (Table 1), while the contribution of $[v_c^\star T_a^\star]$ decreases by about 5%. A harmonic analysis of wavenumber-2 contributions of $v_a^\star$, $T_c^\star$, $v_c^\star$, and $T_a^\star$ shows that the amplitudes of $v_a^\star$ and $T_c^\star$ increase under La Niña conditions and that the phase difference between both remains approximately constant, with both waves still being in phase. These modifications result in a higher correlation between $v_a^\star$ and $T_c^\star$. Although the amplitude of $v_c^\star$ enhances, the phase difference between $v_c^\star$ and $T_a^\star$ also increases, leading to a reduction in the cross correlation. The interaction between both waves decreases. The amount of the single contributions changes after the CD. These results are in agreement with findings in Fig. 2 and give a hint that La Niña climatology has an influence on the amplitude and the phasing of wavenumber-2 anomalies in 2009, which could increase the correlation between $[v_a^\star T_c^\star]$ and reduce the correlation of $[v_c^\star T_a^\star]$. Note that a test of significant differences between La Niña climatology and climatology seems not to be appropriate because both are not independent.

In Fig. 4 the horizontal WAF according to Plumb (1985) and geopotential disturbances are shown. In comparison to climatology, the quasi-stationary planetary wavenumber 2 seems to increase over mid- and high latitudes during climatological La Niña conditions by about 100 m^2 s^{-2} (Figs. 4c and 4f). The difference plot (Fig. 4c) reflects the dominant polar change of wavenumber 1 and the increase of wavenumber-2 amplitude in midlatitudes during La Niña (Fig. 4f). Note that in midlatitudes, the amplitude change of wavenumber 1 is roughly 5 times larger than that of wavenumber 2. During La Niña conditions, the stronger quasi-stationary wave train from the Pacific Ocean over Canada to

TABLE 2. As in Table 1, but the climatology is exchanged by La Niña mean climatology.

Wavenumbers 1–3	$[v^\star T^\star]$	$[v_a^\star T_a^\star]$	%	$[v_c^\star T_c^\star]$	%	$[v_a^\star T_c^\star]$	%	$[v_c^\star T_a^\star]$	%
1–3	59	37	63	13	22	12	20	−3	−5
1	6	4		7		0		−5	
2	55	34	58	5	8	15	25	1	2
3	−2	−1		1		−3		1	

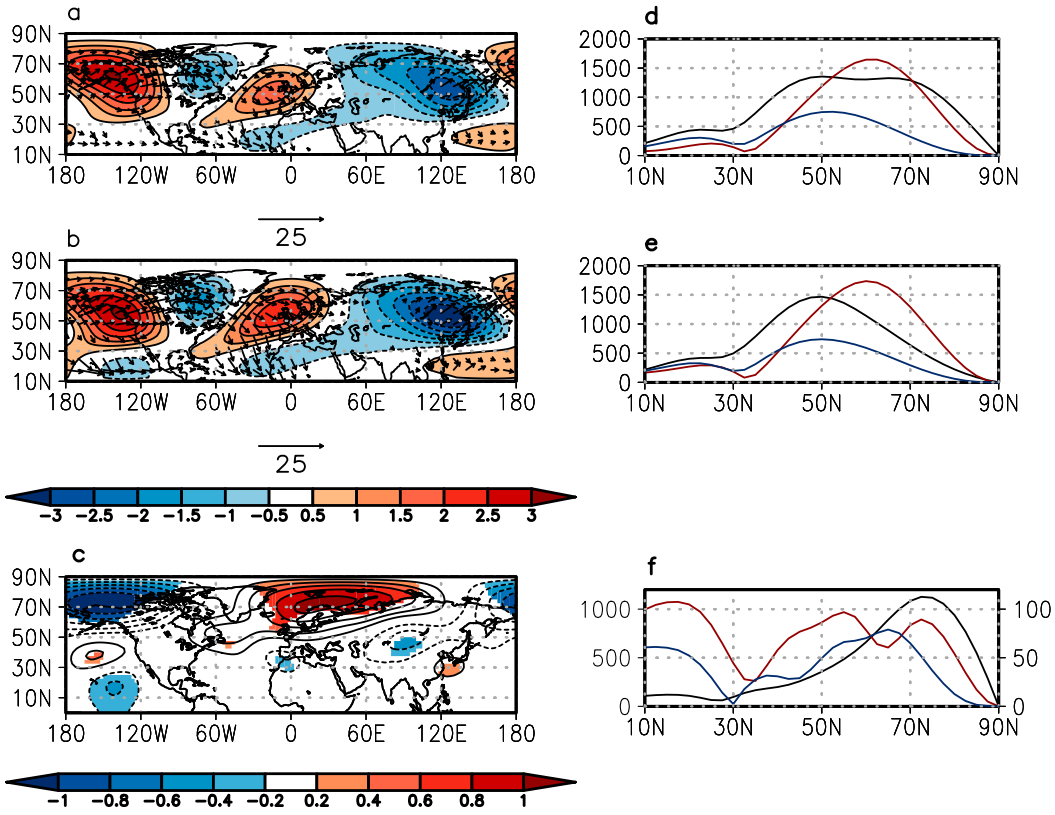

FIG. 4. Cross section of horizontal WAF [$m^2\ s^{-2}$, vectors in (a) and (b)] and geopotential disturbances ($10^3\ m^2\ s^{-2}$, shaded) for (a) climatology (1979–2012), and for (b) the mean La Niña configuration, and (c) the difference between La Niña and ENSO-neutral phase. Shading in (c) indicates statistically significant difference at the 95% confidence level. Quantities are shown for mean January at 100 hPa. The corresponding amplitudes of the geopotential of wavenumber 1 (black), wavenumber 2 (red), and wavenumber 3 (blue) at 100 hPa are shown for (d) climatology, (e) La Niña climatology, and for (f) the difference between La Niña and ENSO-neutral phase. Left *y* axis in (f) is for wavenumber 1 and right *y* axis is for wavenumbers 2 and 3.

northern Europe maintains the anticyclone over the North Atlantic–European region (Fraedrich and Müller 1992). The ridge over Alaska is shifted to the Rockies, and the downstream trough (ridge) over Canada (Scandinavia) is amplified (Fig. 4b).

These results also indicate that for La Niña events in January, the quasi-stationary wave structure is modulated in such a way that the planetary wavenumber 2 is amplified in boreal extratropics and that the planetary wavenumber 1 is weakened in the polar regions of troposphere and lower stratosphere (Fig. 4f).

For January 2009, a similar enhanced poleward wave train is found during the subperiod of 10–6 days before CD, showing the eastward propagation of wave energy from the Alaskan ridge over Canada to the Scandinavian ridge, where it contributes to the maintenance and increase of the ridge (Fig. 5). As the Alaskan ridge weakens and the Scandinavian ridge strengthens (Fig. 3), the contribution of propagating wave activity is weaker in the subperiod of 5–1 day before CD (shown in Fig. S2 in the supplemental material).

In agreement with Ayarzagüena et al. (2011), the first peak in $[v^\star T^\star]$ results mainly (about 58%) from planetary wavenumber-2 anomalies in meridional wind and temperature ($[v_a^\star T_a^\star]$; Table 2) and about 25% comes from the correlation between v_a and T_c La Niña climatology. The quasi-stationary waves are much more amplified during the prephase of MSSW 2009 in comparison to the mean La Niña events. Therefore, an additional forcing must exist in order to force wavenumber 2 in the extratropics.

b. *La Niña and MJO influence on eddies*

The amplified wave 2 in midlatitudes can be associated with two amplified anticyclones. Anticyclones can be maintained against the westerly flow by transient eddies (Shutts 1983). The prephase of MSSW 2009 is characterized by moderate La Niña conditions and by an active MJO in phases 7 and 8 (Fig. S3 in the

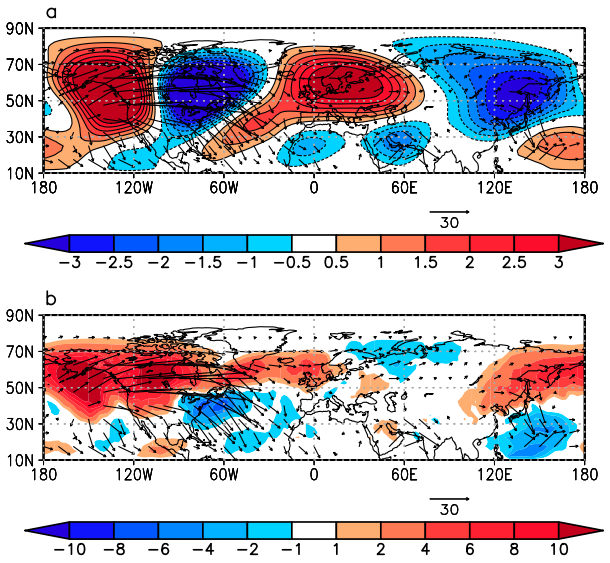

FIG. 5. Cross section of horizontal WAF ($m^2 s^{-2}$, vectors) and (a) geopotential disturbances ($10^3 m^2 s^{-2}$, contours) and (b) vertical component of WAF (contours, $10^{-2} m^2 s^{-2}$) at 100 hPa for the period 10–6 days before CD.

supplemental material). Both La Niña and MJO have an impact on transient eddy activity over the North Pacific (Roundy et al. 2010; Moore et al. 2010; Deng and Jiang 2011). Hence, the cyclone frequency is analyzed as a proxy to quantify the potential La Niña and MJO influences on the wavenumber-2 pattern. Another aspect is the analysis of WCBs, to quantify whether upper-level diabatic outflow is also important for the maintenance of the anticyclone over the North Pacific. If not otherwise stated, these quantities are shown as anomalies from ERA-Interim climatology, related to the considered climatological extended prephase (here: 2–23 January 2009).

During the extended prephase of MSSW 2009, the cyclone frequency exceeded the climatological mean significantly by more than 24% over the central North Pacific (40°–55°N, 160°E–160°W; Fig. 6a) and by 9% over the North Atlantic, but not statistically significant. A similar anomaly structure also holds for La Niña but with a smaller frequency number (Fig. 6b). In particular over the North Pacific, cyclone frequencies are enhanced by more than 15% during La Niña. Likewise, MJO phases 7 and 8 modulate the cyclone activity on shorter time scales, resulting in an increase of cyclone frequency by 6% and 12%, respectively (shown in Fig. S4 in the supplemental material). The North Pacific cyclone frequency is particularly enhanced when MJO phases 7 and 8 and La Niña occur simultaneously (Figs. 6c and 6d). Under these conditions the North Pacific cyclone frequency anomalies exceed 18% and 24% during MJO phases 7 and 8, respectively. Note that the anomaly frequency increase is about one-third larger for MJO active phase 8 in comparison with MJO active phase 7. The co-occurrence of La Niña and MJO phases 7 and 8 during the extended prephase of MSSW 2009 is favorable for anomalously strong cyclone activity over the North Pacific. This result is in agreement with Roundy et al. (2010), showing a strengthening of geopotential anomalies if both La Niña and MJO 7 and 8 are active.

Midlatitude cyclones are associated with strong WCBs, which impact the cyclone itself and the evolution of the downstream flow. The anomalously high cyclone frequency upstream of the positive geopotential anomaly over Alaska during the extended prephase of the MSSW 2009 (Fig. 6a) suggests that WCB activity was anomalously high prior to the MSSW 2009. Thus, we hypothesize that these cross-isentropic airstreams play an important role in the maintenance and strengthening of the ridge over Alaska.

This mechanism is illustrated with a representative example of the prephase (Fig. 7a). On 15 January, the surface flow is characterized by a large low pressure system over the central North Pacific (Fig. 7a). Its mean sea level pressure minimum is collocated with the positive cyclone frequency anomaly during the prephase (cf. Fig. 6a). WCB trajectories start to ascend in subtropical regions to the southeast of the cyclone center on 15 January (Fig. 7a). This stage will be referred to as WCB inflow. The WCB air masses ascend rapidly from the lower to the upper troposphere and reach the crest of a highly amplified downstream ridge over western North America on 17 January. Cross-isentropic ascent within this WCB leads to a transport and injection of subtropical low-PV air into the mid- to high-latitude upper troposphere and contributed, hence, to the maintenance of the existing ridge. This is reflected by PV anomalies of less than −0.7 PVU (1 PVU = $10^{-6} K kg^{-1} m^2 s^{-1}$), which persisted in some parts of the ridge for at least five consecutive days (Fig. 7a).

Occurrence frequency anomalies of trajectories for any stage of the WCB (inflow, ascent, outflow) suggest that WCBs occur frequently just downstream of enhanced cyclone activity during the extended prephase of the MSSW 2009. WCB activity is strongly enhanced in subtropical regions (Fig. 7b) to the southeast of the enhanced cyclone frequency in the central North Pacific (cf. Fig. 6a) and on the upstream flank of the evolving ridge over Alaska, that is, in regions where WCB inflow and outflow are expected, respectively. This enhancement reflects (i) the net transport of subtropical lower-tropospheric low-PV air by WCBs into the crest of the evolving ridge over Alaska and (ii) the recirculation of this low-PV air within the anticyclone, indicating the role of diabatic processes in the maintenance of blocking (Pfahl et al. 2015).

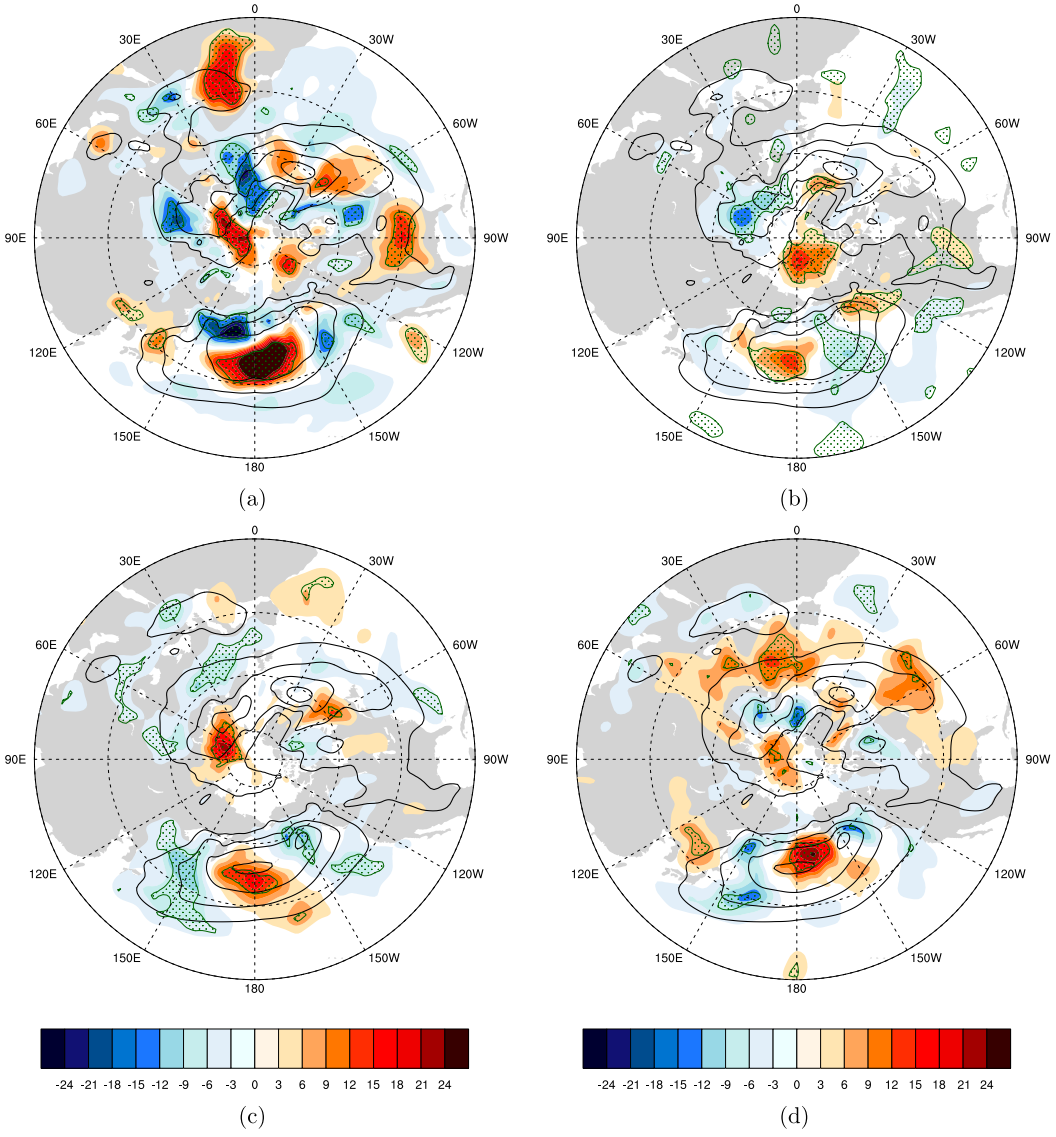

FIG. 6. Cyclone frequency anomaly for (a) the period 2–23 Jan 2009, (b) mean La Niña (also the period 2–23 Jan), and active MJO (c) phase 7 and (d) phase 8 during La Niña with respect to DJF (1980–2010). Isolines indicate the climatology of the respective period in 10% intervals. Shading represents anomalies and green dotted areas indicate statistically significant values at a 95% confidence level from a one-tailed Monte Carlo test using 500 permutations.

In essence, the large-scale conditions set by La Niña and its co-occurrence with MJO phases 7 and 8 provide favorable conditions for increased cyclone frequency over the central North Pacific. During the extended prephase of MSSW 2009, the increased cyclone frequency is associated with an increase of WCB activity over the North Pacific. These WCBs transport subtropical low-PV air into the crest of the evolving Alaskan ridge and contribute to its subsequent maintenance. It should be noted that such an anomalous WCB transport is not found for the Scandinavian ridge. A quantification of the impact of transient eddies on the blocking anticyclones follows in the next subsection.

c. *Maintenance and reinforcement of Alaskan ridge and Scandinavian ridge*

Generally, persistent anticyclones are quasi-stationary disturbances of the zonal flow that are forced mechanically by topography of the continents, thermally by land–sea contrast, and by the divergence of eddy fluxes (Valdes and Hoskins 1989). Their maintenance can be supported by transient eddies, as shown by Shutts (1983) in a linear framework, due to vorticity or "energy transfer" from the

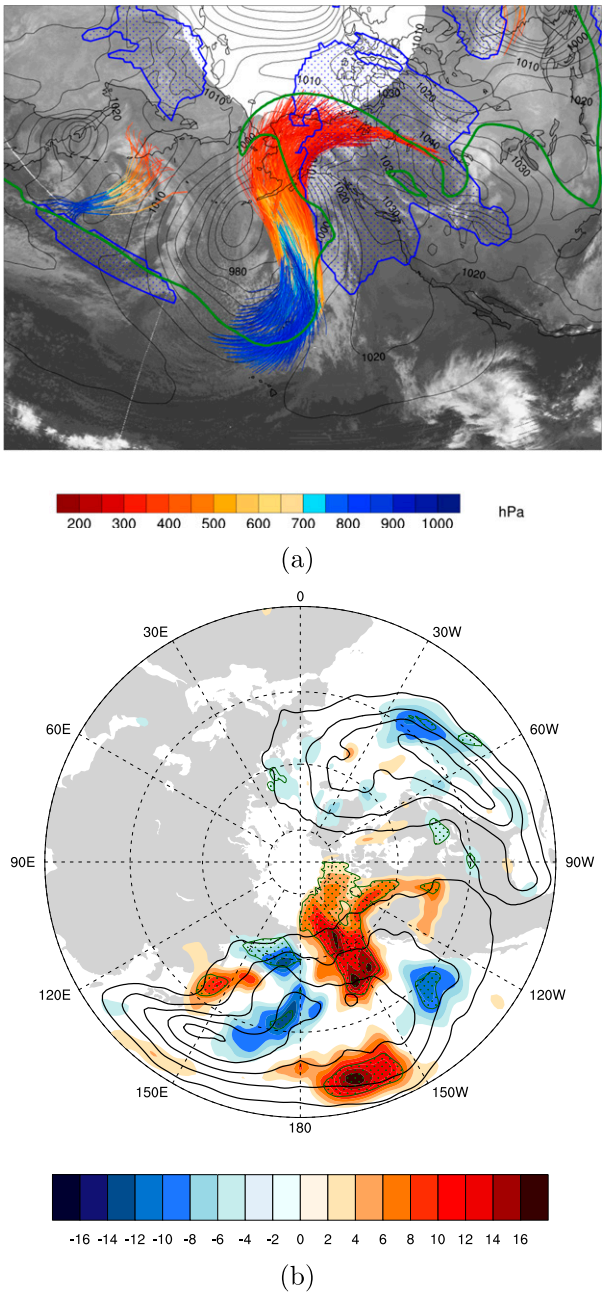

FIG. 7. (a) Representative synoptic situation during the prephase of the MSSW 2009. Mean SLP (black contours, hPa) at 0000 UTC 15 Jan 2009, infrared brightness temperature (shading), 2-PVU contour at 320 K (green contour), and blocking mask (vertically integrated negative PV anomaly, blue stippling) at 0000 UTC 17 Jan 2009. WCB trajectories of 48 h started at 0000 UTC 15 Jan 2009 are colored by pressure. (b) Occurrence frequency anomalies for entire WCBs (t = 0–48 h; shaded every 2%) for 2–23 Jan 2009 and climatological frequency with a 5% contour interval. Statistical significance at the 95% level is shown with green hatching. Fields are smoothed for visualization.

transient eddies to larger scales. Colucci (1987) demonstrated that for the occurrence of a blocking anticyclone, the amplitude of the existing planetary wave and the phase relation of it to the upstream transient eddies are important for the energy transfer. Chen and Van den Dool (1997) have shown that wave trains from the intermediate scale contribute to the maintenance of anticyclone via barotropic energy conversion, which is an additional energy source. Recently, Pfahl et al. (2015) stressed the importance of latent heat release and cross-isentropic transport of air into the upper troposphere for the onset of blocking anticyclones. The following two subsections analyze in more detail which type of Rossby wave trains and which mechanisms are responsible for the maintenance and reinforcement of the two ridges of the MSSW 2009 by using nonlinear approaches of PV and K_e budget analyses.

1) ROSSBY WAVE TRAINS

Three standard time filters [quasi stationary (20–60 days), intermediate (8–20 days), and transient (1–6 days)] are applied in order to examine contributions to wave activity fluxes on different time scales.

(i) Quasi-stationary waves

In comparison to climatology (Fig. 4a), geopotential disturbances (Fig. 5a) are very large in mid- and high latitudes during the prephase. The Alaskan ridge and the Siberian trough (Fig. 5a) roughly match climatological values (Fig. 4a). The Canadian trough and the North Atlantic ridge are strengthened and shifted (Fig. 5a) in comparison to climatology (Fig. 4a). Over and south of Greenland, the northern wave train splits into a northern branch (toward Scandinavia) and into a southern branch (toward the subtropical jet) as shown in Fig. 5. Note that the geopotential disturbances in January 2009 include a dominant wavenumber-2 structure in mid- and high latitudes (Fig. 5a). The evolution of the quasi-stationary waves (Fig. 8) is shown at 100 hPa by using the zonal component of the wave activity flux as a proxy for wave trains (Glatt et al. 2011). Beside some quasi-stationary wave activity at the beginning of the year 2009 (Fig. 8) up to day 9, a quasi-stationary wave train starts over the eastern North Pacific and propagates eastward and upward (not shown) toward the Alaskan ridge and Canadian trough during the extended prephase. This wave train seems to be linked with the weaker North Atlantic–European wave train. Note that these wave trains are weakened after CD.

The analysis reveals that the Alaskan ridge is supported by quasi-stationary waves. The Scandinavian ridge seems to be linked with the Alaskan ridge via quasi-stationary waves, emanating on its western side. These results confirm the studies of Harada et al. (2010) and Ayarzagüena et al. (2011).

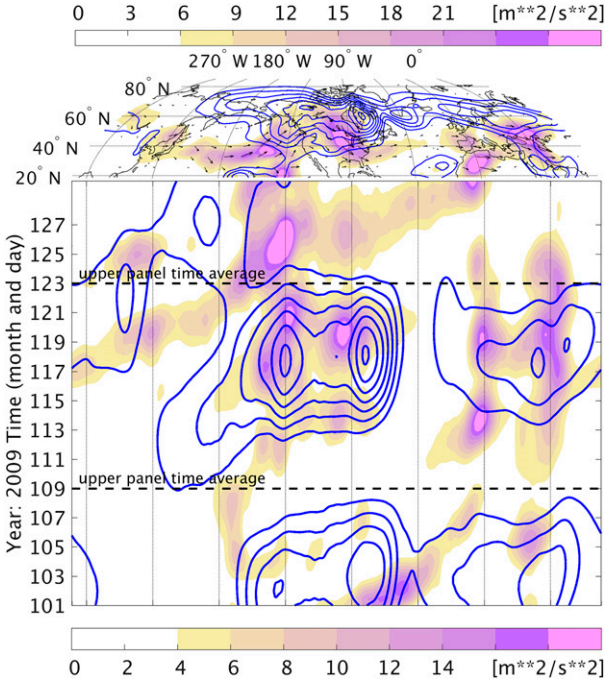

FIG. 8. (bottom) Hovmöller diagram of the zonal component of the wave activity flux for quasi-stationary waves (blue contour) at 100 hPa and for intermediate waves (shaded) at 300 hPa above a threshold of 0 and 5 $m^2 s^{-2}$ for January 2009, respectively, averaged latitudinally from 15° to 80°N. The quasi-stationary wave contribution is defined by a bandpass filter of 20–60 days with a background flow defined by 60 days. The intermediate wave contribution is defined by a bandpass filter of 8–20 days with a background flow defined by 30 days. (top) The quasi-stationary (blue contour) and intermediate (shaded, vectors) wave signals of the wave activity flux averaged over the time span indicated by the horizontal dashed black lines in the Hovmöller diagram.

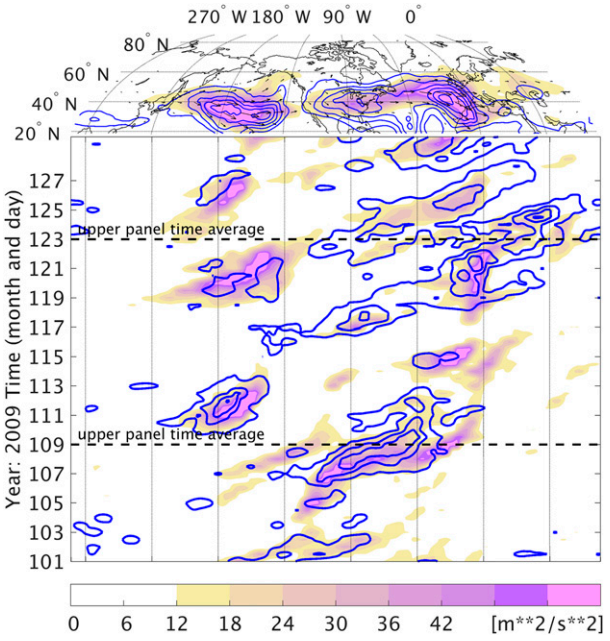

FIG. 9. (bottom) Hovmöller diagram of the zonal component of WAF (fast transient contribution) above a threshold of 0 $m^2 s^{-2}$ (20 $m^2 s^{-2}$) for January 2009 at 100 hPa (blue contour) (at 300 hPa; shaded), averaged latitudinally from 15° to 80°N. The fast transient contribution is defined by a bandpass filter of 1–6 days with a background flow defined by 10 days. (top) The fast transient signal of WAF averaged over the period indicated by the dashed black lines in the Hovmöller diagram. Vectors and shading indicate the fast transients at 300 hPa.

(ii) Intermediate waves

Especially in the extended prephase of January 2009, the intermediate wave trains in the upper troposphere (300 hPa) are enhanced over the North Pacific–North American region, showing that from the central North Pacific intermediate Rossby wave trains are propagating upward (not shown) and eastward over the eastern North Pacific (Fig. 8). West of the Alaskan ridge, the wave activity flux for intermediate waves converges, which reflects the transfer of wave activity from eddies to the anticyclone maintaining the ridge. Note that this wave train intensifies and extends over the North Atlantic after CD. A weaker wave train is found over Europe.

(iii) Transient eddies

In agreement with the increased cyclone frequency over the North Pacific and over the North Atlantic (Fig. 6a, extended prephase), high-pass eddy activity is also strongly increased over the North Pacific and over the North Atlantic during the prephase in the upper troposphere and lower stratosphere (Fig. 9). The comparison with the snapshot of eddy kinetic energy (shown in Fig. 11) shows that the transient eddies reach latitudes north of 60°N over the North Atlantic. In the lower stratosphere (100 hPa), the fast transient eddies emanating from the Alaskan ridge mainly transport energy to the Scandinavian anticyclone (Fig. 9).

In summary, during the prephase all the time-dependent components (quasi stationary, intermediate, and transient) of the spectrum together contribute to the maintenance of both ridges. Especially in the lower stratosphere, the quasi-stationary waves and the transient high-pass eddies seem to be responsible for a far-field impact and link the Alaskan and the Scandinavian anticyclones. In the middle and upper troposphere, the transient high-pass eddy component is stronger, related to the local maintenance on the western flank of the ridges.

2) ERTEL'S POTENTIAL VORTICITY AND EDDY KINETIC ENERGY FRAMEWORKS

To examine the strengthening of the ridge over Alaska independently from wave train filtering, an analysis of

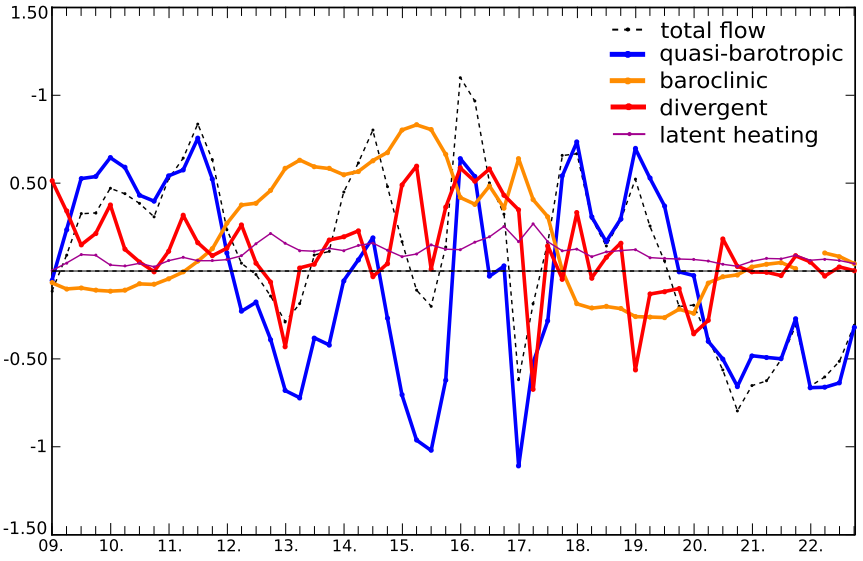

FIG. 10. Time series of the different contributions to the tendency of the integrated PV anomaly (10^8 PVU m^2 s^{-1}). Positive (negative) values indicate strengthening (weakening) of the Alaskan ridge. The colors represent different contributions. PV tendencies are calculated on a 6-hourly basis, starting at 9 Jan 2009 until CD. To account for the vertical variation of the processes, a mean of five isentropic levels (320, 323, 325, 327, 330 K) is chosen.

Ertel's PV balance is applied. This analysis extends the linear theory of Shutts (1983) to nonlinearity, including direct diabatic contributions. Note that this analysis is applied only to the ridge over Alaska, because the Scandinavian ridge was hard to define as a spatially and temporally persistent PV feature during the prephase. Instead, the diagnosis of the K_e budget analysis is applied in order to understand the impact of eddies on the maintenance of the Scandinavian ridge.

(i) PV tendencies

During the extended prephase, two periods of significant amplification of the ridge due to the upper-tropospheric quasi-barotropic wave dynamics occur: during 9–12 January 2009 (−14 to −11 days before CD) and 16–20 January 2009 (−7 to −3 days before CD, with a gap on day 17; Fig. 10). In between, as well as at the end of the prephase, weakening due to the quasi-barotropic contribution is observed. These periods of tendencies with alternating signs can be associated with a synoptic-scale Rossby wave packet that propagates into the western flank of the Alaskan ridge. The baroclinic interaction (bc) contributes to the ridge amplification from 11 to 17 January 2009 (−12 to −6 days before CD), mostly compensating for the negative quasi-barotropic tendencies during this period. Additionally, the ridge is amplified by upper-level divergent flow during most of the considered period, with two periods of prominent amplification: from 9 to 12 January and from 14 to 17 January. Latent heat release makes a further, moderate but constant, contribution to the ridge amplification. The notable role of the divergent flow and of the latent heat release is consistent with the increased WCB frequency noted above (Fig. 7b). The PV diagnostic therefore demonstrates that diabatic processes contribute also to the maintenance or amplification of the Alaskan anticyclone.

(ii) Eddy kinetic energy

In agreement with the WAF analysis above, the period from 8 days before the CD to the CD (despite an interruption on 5 days before the CD) is characterized by episodes of strong K_e flux from the western North Pacific, across the Alaskan ridge, toward the Scandinavian ridge (see Fig. 11 for K_e balance on 8 days before, and Fig. S5 in the supplemental material for K_e balance on 4 days before the CD). The generation of K_e and the chain of adjacent divergence–convergence dipoles of dispersive and advective K_e fluxes along the entire wave train from the western North Pacific to Scandinavia on 15 January 2009 (Fig. 11) illustrates one episode of downstream energy dispersion during the prephase. Note that this clear connection collapses after the CD (not shown). Most of the generation or loss of K_e (Fig. 11a) is attributed to the divergence/convergence of the ageostrophic geopotential flux (Fig. 11b). The starting point for this downstream development is a central North Pacific K_e maximum (30°N, 170°W;

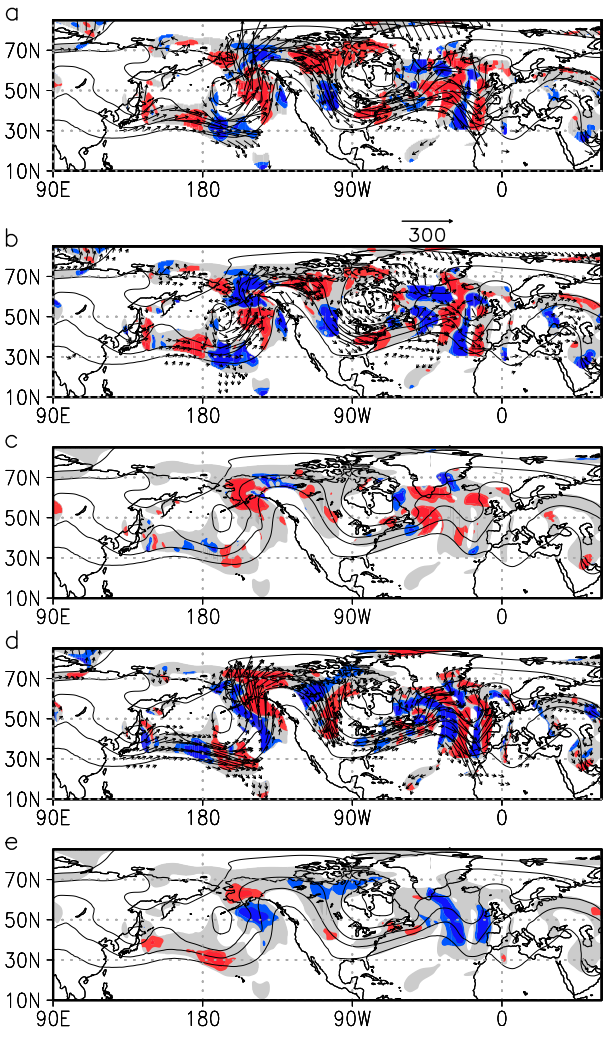

FIG. 11. Eddy kinetic energy budget for 15 Jan 2009 using Eq. (1). The single pictures show the vertical average of K_e (gray shading for values above 10 W m^{-2}), and (a) total tendencies of K_e, (b) divergence/convergence of the ageostrophic geopotential flux, (c) baroclinic conversion, (d) divergence/convergence of the advective flux, and (e) barotropic conversion. Red (blue) shading indicates positive (negative) contributions to the tendency of K_e from a value of 25 (−25) W m^{-2}. Arrows represent the corresponding fluxes: (a) the sum of advective and dispersive K_e flux, (b) dispersive K_e flux, and (d) advective K_e flux.

Fig. 11a) that is associated with the rear flank of a trough that emanated from the western North Pacific around 12 January (not shown). This K_e maximum decays mainly due to the divergence of the ageostrophic geopotential flux (Fig. 11b), which in turn is responsible for the accumulation of energy further downstream along the western flank of the Alaskan ridge. This accumulation is further enhanced by positive baroclinic conversion (Fig. 11c), that is, the ascent of warm air masses along the eastern flank of the central North Pacific trough, which coincides nicely with the positive WCB frequency anomaly. The positive contribution of the advection of K_e by the mean flow in that region (Fig. 11d) indicates that generated K_e is advected farther north into the crest of the ridge. The barotropic conversion is weak (Fig. 11e). East of the Alaskan ridge, positive K_e tendencies are found as a result of the convergence of the ageostrophic geopotential flux (Fig. 11b). This K_e maximum grows, and simultaneously a flux of energy occurs toward the western North Atlantic at roughly 40°N. This strong connection between western North Pacific and North Atlantic is interrupted on 18 January 2009 (not shown). Instead of being directed toward the North Atlantic, K_e is recirculated from the K_e maximum on the eastern side toward the K_e maximum on the western side of the Alaskan ridge. One day later, the connection between the Pacific and Atlantic is reestablished and is clearly visible on 19 January (Fig. S5). North of the subtropical anticyclone over the North Atlantic, which is linked with the Scandinavian ridge, the extratropical cyclone frequency rate is slightly increased (Fig. 6a), but the WCB frequency (Fig. 7b) is not significantly increased. The region of increased cyclone frequency over the North Atlantic is characterized by a K_e flux toward Scandinavia (Fig. 11a)—that means that the Scandinavian ridge is maintained by strong input of K_e from fast transients emanating from the Alaskan ridge, which is directly linked to the western North Pacific (Fig. 8).

4. Summary

In January 2009 a strong MSSW was observed in the Northern Hemisphere. The prephase of MSSW 2009 is characterized by a strong zonal mean eddy heat flux at 100 hPa in the extratropics. The zonal mean eddy heat flux, calculated from ERA-Interim data, can be mainly related to wavenumber-2 components in agreement with earlier studies of Harada et al. (2010) and Ayarzagüena et al. (2011). The maximum of the wavenumber 2–induced zonal mean eddy heat fluxes during the prephase can be explained by anomalously strong meridional flow associated with the amplification of a ridge over both Alaska and Scandinavia. A decomposition of the zonal mean eddy heat flux into the climatological (subscript c, defined as daily climatological mean) and anomalous (subscript a, defined as deviation from climatology) parts shows, in agreement with Ayarzagüena et al. (2011), that the anomalous zonal mean eddy heat flux of the ultralong planetary waves ($[v_a^\star T_a^\star]$) dominates during the prephase. About 61% of the first peak in $[v^\star T^\star]$ stems from the anomalous ultralong waves (59% due to wavenumber 2 alone), and about 20% comes from a $[v_a^\star T_c^\star]$ contribution. If La Niña climatology is considered, then one of the interference terms ($[v_a^\star T_c^\star]$) shows a 5% increase of

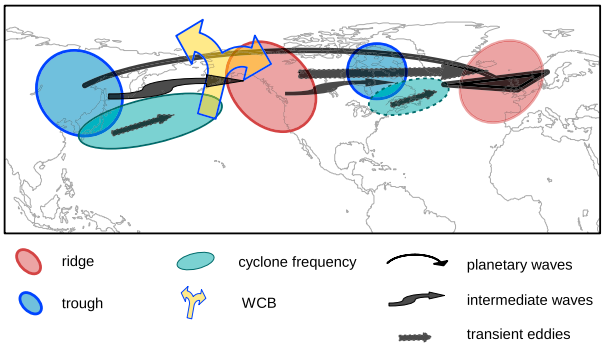

FIG. 12. Scheme of the dominant maintenance and reinforcement of the Alaskan ridge and Scandinavian ridge in the extratropics during the prephase of MSSW 2009. See text for more details.

the contributions of the ultralong wavenumber 2 in the extratropics in comparison to the overall climatology. In general, the comparison between the overall climatology and La Niña climatology shows a strengthening of the quasi-stationary planetary wavenumber 2 in midlatitudes and a weakening of wavenumber 1 in high latitudes during La Niña conditions. The amplification of wavenumber 2 is related to two anticyclones as shown in the schematic Fig. 12.

The decomposition of the zonal mean eddy heat flux shows that the constructive interference terms ($[v_a^\star T_c^\star] + [v_c^\star T_a^\star]$) are of secondary importance for the maximum before the CD, but they play a role. Nishii et al. (2009) analyzed the MSSW event of January 2006, which is dominated by planetary wavenumber 1. For MSSW 2006, the anomalous term also dominates and is above its climatological value ($[v_a^\star T_a^\star]_c$) during two intervals in the prephase of MSSW 2006 (Nishii et al. 2009) but is dominated by planetary wavenumber 1. For both cases, MSSW 2006 and MSSW 2009, the sum of the interaction terms or constructive interference terms ($[v_a^\star T_c^\star] + [v_c^\star T_a^\star]$, amount of 20% for 16–20 January 2009 and an amount of 10% for 16–20 January 2006) is weaker than the anomalous term, but it also contributes. This shows that constructive interference of waves with the climatological planetary waves is important but is secondary.

In addition to moderate La Niña conditions, the extended prephase of the MSSW 2009 coincides with active MJO phases 7 and 8, which tend to precede MSSW events (Garfinkel et al. 2012; Liu et al. 2014). It is shown that the co-occurrence of La Niña and MJO phases 7 and 8 results in a strong (18%) increase of the cyclone frequency in the central North Pacific during the prephase of MSSW 2009. In agreement with the climatological conditions during La Niña and during these MJO phases, the extended prephase is characterized by a significant increase of cyclone frequency (Fig. 12). If the zonal mean eddy heat flux is separately calculated for La Niña and MJO active phases 7 and 8 in winter (DJF, not shown), its contributions sum up to about 16 K m s^{-1} of the total zonal mean eddy heat flux at 100 hPa averaged between 50° and 80°N. More than twice of that is the residual (43 K m s^{-1}) during the subperiod 5–1 day before the CD of MSSW 2009, which remains unexplained. Hence, if only La Niña and MJO active phases 7 and 8 are considered and the influence of other modes is assumed to be small, then the residual is caused by positive feedbacks due to acting MJO during the 2009 La Niña event. Note that as shown in the cyclone frequency analysis, positive feedbacks induced by moderate La Niña and MJO increase strongly the cyclone frequency, which contributes to the maintenance of the anticyclones.

The role of synoptic-scale eddies in communicating the tropical signals to higher latitudes is investigated. The increased cyclone frequency, in line with mean La Niña conditions and active MJO phases 7 and 8, is associated with enhanced WCB activity at the western flank of the Alaskan ridge during the extended prephase (Fig. 12). A positive WCB outflow anomaly is collocated with the ridge over Alaska. This suggests that strong cross-isentropic transport of lower-tropospheric air into the upper troposphere supports the amplification of the ridge over Alaska during the extended prephase of MSSW 2009.

The role of upper-level divergent flow in the amplification and maintenance of the Alaskan ridge is confirmed by the quantitative PV analysis. Furthermore, baroclinic interaction and diabatic PV modification is identified as important contributions to the ridge maintenance.

Eddy kinetic energy flux analysis shows a K_e flux from the western North Pacific, across the ridge over Alaska, toward the Scandinavian ridge, highlighting a teleconnection between the Pacific and Atlantic during the prephase of MSSW 2009. The Scandinavian ridge is mainly maintained by strong input of K_e from Rossby waves that emanate from the Alaskan ridge, propagate over the North Atlantic, and break over Scandinavia as indicated in Fig. 12.

Different time filters [quasi-stationary waves (20–60 days), intermediate waves (8–20 days), and transient eddies (1–6 days)] are applied in order to examine the contributions of Rossby wave trains to wave activity fluxes. In general, during the prephase all time-dependent components of the spectrum contribute to the maintenance of both ridges (indicated wave trains in Fig. 12). In the lower stratosphere, the quasi-stationary waves and the transient high-pass eddies are responsible for the far-field impact and link the Alaskan and the Scandinavian anticyclones. In the middle and upper troposphere, the transient high-pass eddy component is stronger on the western flank of the ridges and also supports their maintenance.

In summary, the present study documents the tropospheric influences during the prephase of MSSW 2009 in four key points: (i) tropical influences of La Niña and MJO are confirmed, (ii) eddy activity in the troposphere links the tropical signals to the high-latitude Alaskan ridge in the North Pacific via enhanced cyclone activity and WCB outflow, (iii) upper-tropospheric wave activity links and strengthens the two ridges during the prephase of MSSW 2009, and (iv) wavenumber-2 amplification by an Alaskan and Scandinavian ridge is shown.

MSSW 2009 is an extraordinary case, showing the importance of the multiscale tropospheric forcing: tropical signals are communicated on different scales and enhance the wavenumber 2–induced zonal mean eddy heat flux in the lower stratosphere at mid- and high latitudes. The present study of MSSW 2009 is an example of how nonlinearity can act. The interaction between ultralong waves and synoptic-scale eddies, and positive feedbacks induced by moderate La Niña and MJO active phases 7 and 8 increase strongly the cyclone frequency that contributes to the maintenance of the anticyclones. As shown above different time scales from transient to quasi stationary and different waves from ultralong to transient eddies maintain and amplify the two anticyclones over Alaska and Scandinavia, thereby causing the increase of the zonal mean eddy heat flux of planetary wavenumber 2.

A sensitivity GCM study with and without La Niña and active MJO would be useful for a better understanding of the specific role of both events in the injection of planetary wave activity into the stratosphere, which is left for future work.

Acknowledgments. This work was supported by the German Science Foundation (DFG, under Grant PE474/7-1/2) and is part of the PANDOWAE project (FOR896, https://www.pandowae.de/). Thanks are given to the Max Planck Institute for Meteorology for the hospitality and to Klaus Fraedrich, where AS is a guest in his fellow group. We thank Deutscher Wetterdienst for providing access to the ECMWF reanalysis, ERA-Interim, and YOTC data. We thank the Atmospheric Dynamics group at ETH Zürich—namely, Hanin Binder, Maxi Böttcher, Anne Kunz, Erica Madonna, Lukas Papritz, Stephan Pfahl, and Michael Sprenger—for helping with the investigation of synoptic weather systems. The contribution of CMG was supported by the Swiss National Science Foundation (SNSF) under Grant PZ00P2_141777/1. The authors thank three anonymous reviewers for the helpful comments and constructive suggestions, which helped to improve the manuscript.

REFERENCES

Albers, J. R., and T. Birner, 2014: Vortex preconditioning due to planetary and gravity waves prior to sudden stratospheric warmings. *J. Atmos. Sci.*, **71**, 4028–4054, doi:10.1175/JAS-D-14-0026.1.

Andrews, D. G., J. R. Holton, and C. B. Leovy, 1987: *Middle Atmosphere Dynamics.* International Geophysics Series, Vol. 40, Academic Press, 489 pp.

Ayarzagüena, B., U. Langematz, and E. Serrano, 2011: Tropospheric forcing of the stratosphere: A comparative study of the two different major stratospheric warmings in 2009 and 2010. *J. Geophys. Res.*, **116**, D18114, doi:10.1029/2010JD015023.

Barriopedro, D., and N. Calvo, 2014: On the relationship between ENSO, stratospheric sudden warmings, and blocking. *J. Climate*, **27**, 4704–4720, doi:10.1175/JCLI-D-13-00770.1.

Butler, A. H., and L. M. Polvani, 2011: El Niño, La Niña, and stratospheric sudden warmings: A reevaluation in light of the observational record. *Geophys. Res. Lett.*, **38**, L13807, doi:10.1029/2011GL048084.

——, D. J. Seidel, S. C. Hardiman, N. Butchart, T. Birner, and A. Match, 2015: Defining sudden stratospheric warmings. *Bull. Amer. Meteor. Soc.*, **96**, 1913–1928, doi:10.1175/BAMS-D-13-00173.1.

Carlson, T., 1980: Airflow through midlatitude cyclones and the comma cloud pattern. *Mon. Wea. Rev.*, **108**, 1498–1509, doi:10.1175/1520-0493(1980)108<1498:ATMCAT>2.0.CO;2.

Charney, J. G., and P. G. Drazin, 1961: Propagation of planetary-scale disturbances from the lower into the upper atmosphere. *J. Geophys. Res.*, **66**, 83–109, doi:10.1029/JZ066i001p00083.

Chen, W. Y., and H. M. Van den Dool, 1997: Asymmetric impact of tropical SST anomalies on atmospheric internal variability over the North Pacific. *J. Atmos. Sci.*, **54**, 725–740, doi:10.1175/1520-0469(1997)054<0725:AIOTSA>2.0.CO;2.

Colucci, S. J., 1987: Comparative diagnosis of blocking versus nonblocking planetary-scale circulation changes during synoptic-scale cyclogenesis. *J. Atmos. Sci.*, **44**, 124–139, doi:10.1175/1520-0469(1987)044<0124:CDOBVN>2.0.CO;2.

Davis, C. A., M. T. Stoelinga, and Y.-H. Kuo, 1993: The integrated effect of condensation in numerical simulations of extratropical cyclones. *Mon. Wea. Rev.*, **121**, 2309–2330, doi:10.1175/1520-0493(1993)121<2309:TIEOCI>2.0.CO;2.

Dee, D. P., and Coauthors, 2011: The ERA-Interim reanalysis: Configuration and performance of the data assimilation system. *Quart. J. Roy. Meteor. Soc.*, **137**, 553–597, doi:10.1002/qj.828.

Deng, Y., and T. Jiang, 2011: Intraseasonal modulation of the North Pacific storm track by tropical convection in boreal winter. *J. Climate*, **24**, 1122–1137, doi:10.1175/2010JCLI3676.1.

Dickinson, R. E., 1969: Vertical propagation of planetary Rossby waves through an atmosphere with Newtonian cooling. *J. Geophys. Res.*, **74**, 929–938, doi:10.1029/JB074i004p00929.

Edmon, H. J., Jr., B. J. Hoskins, and M. E. McIntyre, 1980: Eliassen-Palm cross sections for the troposphere. *J. Atmos. Sci.*, **37**, 2600–2616, doi:10.1175/1520-0469(1980)037<2600:EPCSFT>2.0.CO;2.

Ertel, H., 1942: Ein neuer hydrodynamischer Erhaltungssatz. *Meteor. Z.*, **30**, 543–544.

Ferranti, L., T. N. Palmer, F. Molteni, and E. Klinker, 1990: Tropical-extratropical interaction associated with the 30-60 day oscillation and its impact on medium and extended range prediction. *J. Atmos. Sci.*, **47**, 2177–2199, doi:10.1175/1520-0469(1990)047<2177:TEIAWT>2.0.CO;2.

Fraedrich, K., and K. Müller, 1992: Climate anomalies in Europe associated with ENSO extremes. *Int. J. Climatol.*, **12**, 25–31, doi:10.1002/joc.3370120104.

Garfinkel, C. I., S. B. Feldstein, D. W. Waugh, C. Yoo, and S. Lee, 2012: Observed connection between stratospheric sudden warmings and the Madden-Julian Oscillation. *Geophys. Res. Lett.*, **39**, L18807, doi:10.1029/2012GL053144.

——, J. J. Benedict, and E. D. Maloney, 2014: Impact of the MJO on the boreal winter extratropical circulation. *Geophys. Res. Lett.*, **41**, 6055–6062, doi:10.1002/2014GL061094.

Glatt, I., A. Dörnbrack, S. Jones, J. Keller, O. Martius, A. Müller, D. H. W. Peters, and V. Wirth, 2011: Utility of Hovmöller diagrams to diagnose Rossby wave trains. *Tellus*, **63A**, 991–1006, doi:10.1111/j.1600-0870.2011.00541.x.

Grams, C. M., and H. M. Archambault, 2016: The key role of diabatic outflow in amplifying the midlatitude flow: A representative case study of weather systems surrounding western North Pacific extratropical transition. *Mon. Wea. Rev.*, **144**, 3847–3869, doi:10.1175/MWR-D-15-0419.1.

——, and Coauthors, 2011: The key role of diabatic processes in modifying the upper-tropospheric wave guide: A North Atlantic case-study. *Quart. J. Roy. Meteor. Soc.*, **137**, 2174–2193, doi:10.1002/qj.891.

Harada, Y., A. Goto, H. Hasegawa, N. Fujikawa, H. Naoe, and T. Hirooka, 2010: A major stratospheric sudden warming event in January 2009. *J. Atmos. Sci.*, **67**, 2052–2069, doi:10.1175/2009JAS3320.1.

Hinssen, Y., A. van Delden, and T. Opsteegh, 2011: Influence of sudden stratospheric warmings on tropospheric winds. *Meteor. Z.*, **20**, 259–266, doi:10.1127/0941-2948/2011/0503.

Hitchcock, P., T. G. Shepherd, and G. L. Manney, 2013: Statistical characterization of Arctic polar-night jet oscillation events. *J. Climate*, **26**, 2096–2116, doi:10.1175/JCLI-D-12-00202.1.

Holton, J. R., 1992: *An Introduction to Dynamic Meteorology*. 3rd ed. Academic Press, 511 pp.

Hoskins, B. J., M. E. McIntyre, and A. W. Robertson, 1985: On the use and significance of isentropic potential vorticity maps. *Quart. J. Roy. Meteor. Soc.*, **111**, 877–946, doi:10.1002/qj.49711147002.

Labitzke, K., 1987: Sunspots, the QBO, and the stratospheric temperature in the north polar region. *Geophys. Res. Lett.*, **14**, 535–537, doi:10.1029/GL014i005p00535.

——, and M. Kunze, 2009: On the remarkable Arctic winter in 2008/2009. *J. Geophys. Res.*, **114**, D00I02, doi:10.1029/2009JD012273.

Liu, C., B. Tian, K.-F. Li, G. L. Manney, N. J. Livesey, Y. L. Yung, and D. E. Waliser, 2014: Northern Hemisphere mid-winter vortex-displacement and vortex-split stratospheric sudden warmings: Influence of the Madden-Julian Oscillation and Quasi-Biennial Oscillation. *J. Geophys. Res. Atmos.*, **119**, 12 599–12 620, doi:10.1002/2014JD021876.

Madonna, E., H. Wernli, H. Joos, and O. Martius, 2014: Warm conveyor belts in the ERA-Interim dataset (1979–2010). Part I: Climatology and potential vorticity evolution. *J. Climate*, **27**, 3–26, doi:10.1175/JCLI-D-12-00720.1.

Martius, O., L. M. Polvani, and H. C. Davies, 2009: Blocking precursors to stratospheric sudden warming events. *Geophys. Res. Lett.*, **36**, L14806, doi:10.1029/2009GL038776.

Matsuno, T., 1971: A dynamical model of the stratospheric sudden warming. *J. Atmos. Sci.*, **28**, 1479–1494, doi:10.1175/1520-0469(1971)028<1479:ADMOTS>2.0.CO;2.

Moore, R. W., O. Martius, and T. Spengler, 2010: The modulation of the subtropical and extratropical atmosphere in the Pacific basin in response to the Madden–Julian oscillation. *Mon. Wea. Rev.*, **138**, 2761–2779, doi:10.1175/2010MWR3194.1.

Newman, P. A., E. R. Nash, and J. E. Rosenfield, 2001: What controls the temperature of the Arctic stratosphere during the spring? *J. Geophys. Res.*, **106**, 19 999–20 010, doi:10.1029/2000JD000061.

Nishii, K., H. Nakamura, and T. Miyasaka, 2009: Modulations in the planetary wave field induced by upward-propagating Rossby wave packets prior to stratospheric sudden warming events: A case-study. *Quart. J. Roy. Meteor. Soc.*, **135**, 39–52, doi:10.1002/qj.359.

Orlanski, I., and J. Katzfey, 1991: The life cycle of a cyclone wave in the Southern Hemisphere. Part I: Eddy energy budget. *J. Atmos. Sci.*, **48**, 1972–1998, doi:10.1175/1520-0469(1991)048<1972:TLCOAC>2.0.CO;2.

——, and J. P. Sheldon, 1995: Stages in the energetics of baroclinic systems. *Tellus*, **47A**, 605–628, doi:10.1034/j.1600-0870.1995.00108.x.

Pedatella, N. M., and Coauthors, 2014: The neutral dynamics during the 2009 sudden stratosphere warming simulated by different whole atmosphere models. *J. Geophys. Res. Space Phys.*, **119**, 1306–1324, doi:10.1002/2013JA019421.

Peters, D. H. W., A. Schneidereit, M. Bügelmayer, C. Zülicke, and I. Kirchner, 2015: Atmospheric circulation changes in response to an observed zonal ozone anomaly. *Atmos.–Ocean*, **53**, 74–88, doi:10.1080/07055900.2013.878833.

Pfahl, S., and H. Wernli, 2012: Quantifying the relevance of cyclones for precipitation extremes. *J. Climate*, **25**, 6770–6780, doi:10.1175/JCLI-D-11-00705.1.

——, C. Schwierz, M. Croci-Maspoli, C. M. Grams, and H. Wernli, 2015: Importance of latent heat release in ascending air streams for atmospheric blocking. *Nat. Geosci.*, **8**, 610–614, doi:10.1038/ngeo2487.

Piaget, N., P. Froidevaux, P. Giannakaki, F. Gierth, O. Martius, M. Riemer, G. Wolf, and C. M. Grams, 2015: Dynamics of a local Alpine flooding event in October 2011: Moisture source and large-scale circulation. *Quart. J. Roy. Meteor. Soc.*, **141**, 1922–1937, doi:10.1002/qj.2496.

Plumb, R. A., 1985: On the three-dimensional propagation of stationary waves. *J. Atmos. Sci.*, **42**, 217–229, doi:10.1175/1520-0469(1985)042<0217:OTTDPO>2.0.CO;2.

Polvani, L. M., and D. W. Waugh, 2004: Upward wave activity flux as a precursor to extreme stratospheric events and subsequent anomalous surface weather regimes. *J. Climate*, **17**, 3548–3554, doi:10.1175/1520-0442(2004)017<3548:UWAFAA>2.0.CO;2.

Riemer, M., M. Baumgart, and S. Eiermann, 2014: Cyclogenesis downstream of extratropical transition analyzed by **Q**-vector partitioning based on flow geometry. *J. Atmos. Sci.*, **71**, 4204–4220, doi:10.1175/JAS-D-14-0023.1.

Roundy, P. E., K. MacRitchie, J. Asuma, and T. Melino, 2010: Modulation of the global atmospheric circulation by combined activity in the Madden–Julian oscillation and the El Niño–Southern Oscillation during boreal winter. *J. Climate*, **23**, 4045–4059, doi:10.1175/2010JCLI3446.1.

Shutts, G. J., 1983: The propagation of eddies in diffluent jetstreams: Eddy vorticity forcing of 'blocking' flow fields. *Quart. J. Roy. Meteor. Soc.*, **109**, 737–761, doi:10.1002/qj.49710946204.

Simmons, A. J., and B. J. Hoskins, 1979: The downstream and upstream development of unstable baroclinic waves. *J. Atmos. Sci.*, **36**, 1239–1254, doi:10.1175/1520-0469(1979)036<1239:TDAUDO>2.0.CO;2.

Sprenger, M., and H. Wernli, 2015: The LAGRANTO Lagrangian analysis tool - version 2.0. *Geosci. Model Dev.*, **8**, 2569–2586, doi:10.5194/gmd-8-2569-2015.

Takaya, K., and H. Nakamura, 1997: A formulation of a wave-activity flux for stationary Rossby waves on a zonally varying basic flow. *Geophys. Res. Lett.*, **24**, 2985–2988, doi:10.1029/97GL03094.

Teubler, F., and M. Riemer, 2016: Dynamics of Rossby wave packets in a quantitative potential vorticity potential temperature framework. *J. Atmos. Sci.*, **73**, 1063–1081, doi:10.1175/JAS-D-15-0162.1.

Tripathi, O. P., and Coauthors, 2015: The predictability of the extratropical stratosphere on monthly time-scales and its impact on the skill of tropospheric forecasts. *Quart. J. Roy. Meteor. Soc.*, **141**, 987–1003, doi:10.1002/qj.2432.

Valdes, P. J., and B. J. Hoskins, 1989: Linear stationary wave simulations of the time-mean climatological flow. *J. Atmos. Sci.*, **46**, 2509–2527, doi:10.1175/1520-0469(1989)046<2509:LSWSOT>2.0.CO;2.

van Loon, H., and K. Labitzke, 1987: The Southern Oscillation. Part V: The anomalies in the lower stratosphere of the Northern Hemisphere in winter and a comparison with the quasi-biennial oscillation. *Mon. Wea. Rev.*, **115**, 357–369, doi:10.1175/1520-0493(1987)115<0357:TSOPVT>2.0.CO;2.

Waugh, D. W., W. J. Randel, S. Pawson, P. A. Newman, and E. R. Nash, 1999: Persistence of the lower stratospheric polar vortices. *J. Geophys. Res.*, **104**, 27 191–27 201, doi:10.1029/1999JD900795.

Wernli, H., and C. Schwierz, 2006: Surface cyclones in the ERA-40 dataset (1958–2001). Part I: Novel identification method and global climatology. *J. Atmos. Sci.*, **63**, 2486–2507, doi:10.1175/JAS3766.1.

Wheeler, M. C., and H. H. Hendon, 2004: An all-season real-time multivariate MJO index: Development of an index for monitoring and prediction. *Mon. Wea. Rev.*, **132**, 1917–1932, doi:10.1175/1520-0493(2004)132<1917:AARMMI>2.0.CO;2.